J Sol-Gel Sci Technol
DOI 10.1007/s10971-011-2650-1

ORIGINAL PAPER

Magnetic Fe doped ZnO nanofibers obtained by electrospinning

Anna Baranowska-Korczyc · Anna Reszka · Kamil Sobczak · Bożena Sikora · Piotr Dziawa · Marta Aleszkiewicz · Łukasz Kłopotowski · Wojciech Paszkowicz · Piotr Dłużewski · Bogdan J. Kowalski · Tomasz A. Kowalewski · Maciej Sawicki · Danek Elbaum · Krzysztof Fronc

Received: 8 August 2011 / Accepted: 5 December 2011

Abstract We demonstrate structural and room temperature magnetic properties of Fe doped ZnO nanofibers (NFs) obtained by electrospinning followed by calcination. The observed NFs, formed from crystalographically oriented, approximately 4.5 nm particles conglomerates, were approximately 200 nm in diameter. The reported synthesis of room temperature ferromagnetic Fe doped ZnO NFs is both facile and economical, and is therefore suggested as a generic method of fabricating biocompatible magnetic materials. The major substrates selected for the NFs synthesis (Zn, Fe) comprised of relatively low toxicity materials. Incorporating 10% Fe into ZnO does not modify the wurtzite crystal structure of the host material. No evidence of impurity phase was detected by either X-ray or electron diffraction. Magnetometry studies and Magnetic Force Microscopy imaging reveal a local ferromagnetic order that persists up to room temperature. We suggest that the observed phenomenon is either due to a mechanism mediated by presence of oxygen vacancies and/or is related to iron-rich precipitates.

Keywords Electrospinning · ZnO nanofibers · ZnFeO · Room temperature ferromagnetism · Magnetic oxides

A. Baranowska-Korczyc (✉) · A. Reszka · K. Sobczak · B. Sikora · P. Dziawa · M. Aleszkiewicz · Ł. Kłopotowski · W. Paszkowicz · P. Dłużewski · B. J. Kowalski · M. Sawicki · D. Elbaum · K. Fronc
Institute of Physics, Polish Academy of Sciences, al. Lotników 32/46, 02668 Warsaw, Poland
e-mail: akorczyc@ifpan.edu.pl

T. A. Kowalewski
Institute of Fundamental Technology Research, Polish Academy of Sciences, ul. Pawińskiego 5B, 02106 Warsaw, Poland

1 Introduction

The physical origin and the occurrence of ZnO doped with transition metal cations ferromagnetism are subject to active research. In spite of numerous studies the ferromagnetic properties of transition metal cations doped wurtzite ZnO host is still a controversial issue [1–6]. A high temperature ferromagnetism was reported numerously for Co doped ZnO in thin films produced by all accessible methods including pulsed layer deposition [7], the magnetron co-sputtering [8], the sol–gel method [9], and epitaxial thin films [10]. Recently, Fe doped ZnO nanostructures, synthesized by the sol–gel method, were observed to be ferromagnetic [11]. The observed room temperature ferromagnetism was reported to be an intrinsic Fe doped ZnO property. Interestingly, neither Fe, nor FeO and Fe_2O_3 phase in the Fe doped ZnO nanoparticles were observed based on X-ray absorption near edge structure measurements [11]. On the other hand, there are report claiming no essential role of the transition metals in the ZnO magnetism in low dimension Fe and Mn doped ZnO films [12]. In particular, based on the magnetic properties of Mn doped ZnO layers, after subtraction of the substrate effects, no evidence of a sample ferromagnetism was observed [13]. Both reports point that a significant contribution to the room temperature ferromagnetism comes from the surface and/or the interface defects located between the sample and substrate. Interestingly, ferromagnetism has been also reported in thin films and nanoparticles of a large family of undoped wide gap semiconductors (ZnO, TiO_2, HfO_2, SnO_2, etc.) [3]. The ferromagnetism observed in the semiconductor nanostructures was attributed to oxygen defects which are of special significance in low dimension samples [14]. Additionally, based on a study of laser-deposited thin films of $Zn_{1-x}Co_xO$, the antiferromagnetic super exchange interaction was proposed to be the dominant mechanism for the exchange coupling between Co

Published online: 17 December 2011

and $Zn_{1-x}Co_xO$ [15]. Similar explanation was provided for polycrystalline powders synthesized by two different methods: solid-state and liquid-phase reactions [16]. The above observations have their foundation in calculations of the local spin density functional theory for $Zn_{1-x}Co_x$ [6]. The authors observed that the dominant magnetic interaction in well-characterized stochiometric phase (x up to 0.15) is dominated by the near neighbour antiferromagnetic coupling and these calculations suggested that ferromagnetism will only occur in the presence of additional hole doping. Based on similar calculations a short range nature of ferromagnetic and antiferromagnetic interactions was observed and a spin-glass like state was noted based on energy considerations for Co doped ZnO [17]. Recently, defect induced Fe doped ZnO reversible ferromagnetism was reported and attributed to hydrogen mediated oxygen vacancies [18]. Similarly, ferromagnetic Co doped ZnO was reported and reversible manipulation of short-range spin ordering by injection and ejection of hydrogen was demonstrated [19].

1D semiconductor nanostructures such as wires, tubes, belts and fibers have attracted a great deal of attention in recent years. Among many techniques, which allow to obtain 1D semiconductors, electrospinning is one of the most simple, versatile, low-cost, and effective. The method has an attractive potential for producing NFs from polymers, composites or ceramics with diameters ranging from tens of nanometers to microns [20–24]. Moreover, NFs length is limited only by the stability of process parameters, time, and amount of applied material [23, 24]. In particular, electrospinning, followed by calcination, is a versatile way to synthesize ZnO nanofibers [25–27]. The nanofibers consist of conglomerates of nanostructured polycrystalline domains, which are responsible for their very large surface to volume ratio. ZnO doped with transition metal ions such as Co, Mn, Ni or Fe is a promising candidate for a room temperature ferromagnetic semiconductor [28]. Additionally, combining the ability to form NFs with transition metal doping makes the electrospinning a very promising method for providing magnetic nanofibers with potential applications in magnetic sensors, flexible magnets and biosensors.

In this study, we demonstrate the feasibility of obtaining Fe doped ZnO nanofibers exhibiting ferromagnetism above room temperature. We show that the ferromagnetic signal derives from a collective behavior typical for a blocked super paramagnet and estimate the size of nano crystallites which form the blocked state. We point out that incorporating 10% Fe into ZnO in electrospun materials does not lead to sizeable precipitates of other impurity phases and discuss possible origins of the ferromagnetic coupling. The synthesized material is non toxic thus could have potential biomedical applications [29–31].

2 Experimental

2.1 Electrospinning and calcinations

We prepared undoped and iron doped ZnO nanofibers by a procedure, which consisted of four steps. The first step was to obtain 10% (wt) solution of poly(vinyl alcohol) (PVA, $M_W = 72{,}000$) $(C_2H_4)_n$ (POCH, Poland) in deionized water (0.08 μS). Aqueous solution of PVA was prepared by keeping the mixture at 60 °C for 7 days. The second step was a sol–gel process, 0.25 g of zinc acetate dihydrate ($Zn(CH_3COO)_2{\cdot}2H_2O$) (CHEMPUR, Poland) was dissolved in 1.25 g solution of PVA as a precursor to obtain ZnO nanofibers. Fe doping was realized by adding 0.022 g iron acetate $(CH_3CO_2)_2Fe$ (Sigma Aldrich) to the mixture. The atomic ratio of Fe to Zn ions was about 0.1. The following step was the electrospinning process. The flow rate was stabilized at 0.2 ml/h by a syringe pump (Ascor S.A., AP12). The electric potential applied between the tip of the needle and the grounded collector placed 15 cm below was equal to 30 kV. In order to produce uniaxially oriented fibers for magnetometric studies, we employed a collector consisting of two separated bars of a conductive material [32]. The fibers were formed at 22 °C and humidity in the range from 30 to 40%. The last step to form ZnO was the NFs calcination in air, at 500 °C for 4 h.

2.2 Characterization

Structural characterization of NFs was performed by X-ray diffraction (XRD) and transmission electron microscopy (TEM). A high-resolution powder diffractometer (Philips X'Pert MPD Pro Alpha1) employing $CuK\alpha_1$ radiation was used. The Bragg–Brentano geometry of the apparatus was modified by monochromatizing the incident beam using a Johansson Ge (111) monochromator. For detection, a linear semiconductor strip detector was used. The data were collected for 12 h. TEM and electron diffraction images were obtained on a JEM2000EX electron transmission microscope at an accelerating voltage of 200 kV.

Scanning electron microscopy (SEM) provided information on NFs morphology. SEM images were obtained on Hitachi SU-70 microscope at an accelerating voltage of 5 kV. Chemical composition was investigated by energy dispersive X-ray spectroscopy (EDX) with incident beam current 6.5 nA and accelerating voltage 15 kV (Thermo Scientific Ultra Dry). Light emission properties were probed by cathodoluminescence (CL) (Gatan MonoCl-3) with beam accelerating voltage of 15 keV and incident current of 6.5 nA. To gain general information about the magnetic properties, the Fe doped ZnO fibers were investigated using superconducting quantum interference device (SQUID) magnetometry at temperatures ranging from 2 K up to

room temperature. Magnetic Force Microscopy (MFM) (Veeco, Nanoscope IIIa MultiMode with standard MESP-type tip) was applied to image the magnetic signal at room temperature. Prior to MFM the atomic force microscopy (AFM) in tapping mode (Nanoscope IIIa with OTESPA 160 μm tip) was used to check the vertical corrugations of the deposited fibers. MFM was performed in lift mode with lift height 150 nm, above the diameter of the thickest fibers.

3 Results and discussion

SEM images show entwined NFs with diameters in the range from 100 to 500 nm and suggest that NFs consist of nanometer size crystallites (Fig. 1). The XRD patterns (Fig. 2) of both undoped and Fe doped ZnO nanofibers exhibit peaks revealing their wurtzite structure [33]. No additional peaks are found in the spectra of Fe doped NFs suggesting an absence of sizable precipitates of Fe-rich phases. This observation is supported by TEM investigations. The electron diffraction patterns, shown in Fig. 3, correspond to the wurtzite structure of ZnO [33]. No evident differences in the diffraction rings were noted pointing out that the doping does not affect the crystalline structure. Importantly, TEM images confirm that the NFs are indeed built as conglomerates of nanocrystallites. The crystal diameters were obtained from dark field TEM images (example inset in Fig. 4a, b). The size distributions for the undoped and Fe doped samples are shown in Fig. 4. For both samples we find average grain size of about 4.5 nm. We did not observed the second phase crystal with

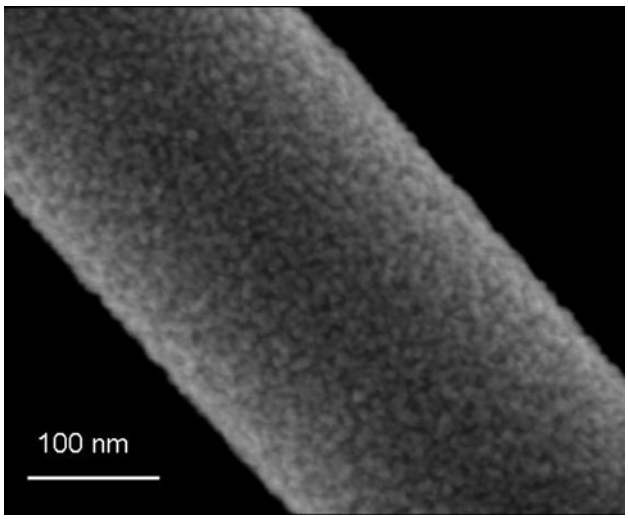

Fig. 1 SEM image of the Fe doped ZnO nanofiber showing that is formed by the conglomerates of nanocrystallites few nanometer in diameter

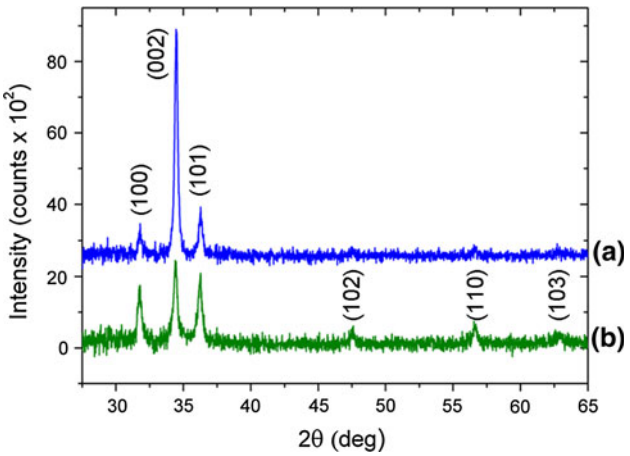

Fig. 2 XRD patterns of ZnO nanofibers: undoped (*a*) and Fe doped (*b*). The top spectrum is shifted by 2,500 counts for clarity

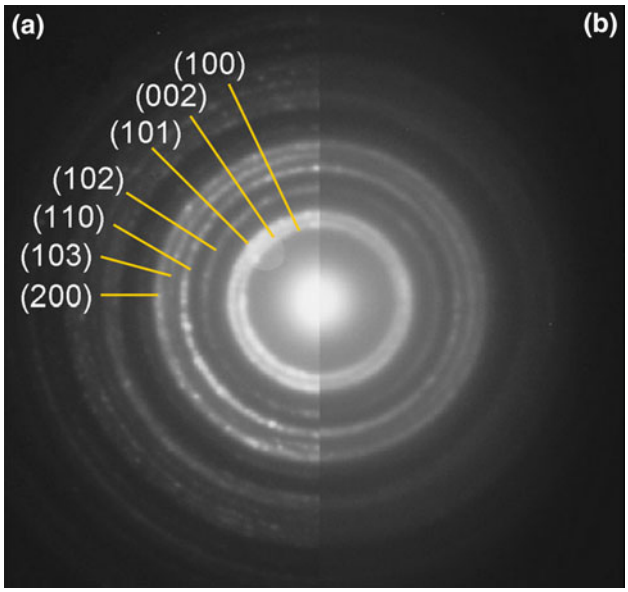

Fig. 3 Electron diffraction pattern of ZnO nanofibers, undoped (**a**) and Fe doped (**b**)

different sizes for Fe doped NFs. The orientation of the nanocrystallites can be inferred from the intensities of XRD and electron diffraction patterns. Among the XRD peaks, the strongest ones are those corresponding to 002 planes (Fig. 2). Moreover, the intensities of electron diffraction rings are not uniform azimuthally (Fig. 3). Both results point out that nanocrystallites are preferentially oriented with the 001 direction perpendicular to the fiber axis.

Chemical characterization was performed by EDX analysis, which confirmed the intended chemical composition of the fibers after electrospinning and calcinations processes. Indeed, a standardless quantitative analysis

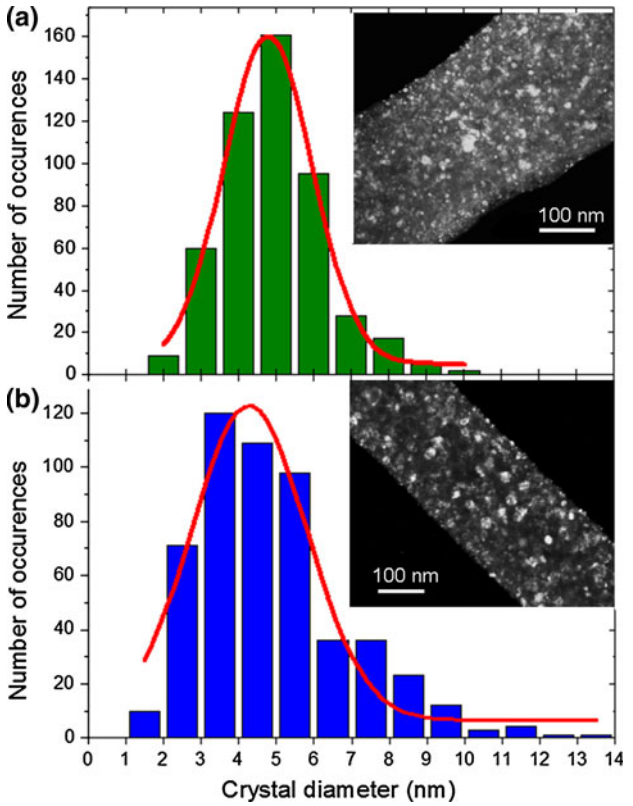

Fig. 4 Crystal size distribution of: Fe doped (**a**) and undoped ZnO nanofibers (**b**) obtained from the TEM measurements. The *dark* field images: Fe doped (**a**) and undoped (**b**) ZnO nanofibers, respectively (*inset*)

yielded Fe/Zn ratio equal to 0.095 (±0.012). Moreover, the cross-section analysis of a doped sample shows that iron dopant atoms are homogeneously distributed across the nanofibers (Fig. 5). Thus, the EDX analysis supports the conclusion about an absence of sizable Fe aggregations inside the bulk of the Fe doped ZnO nanofibers.

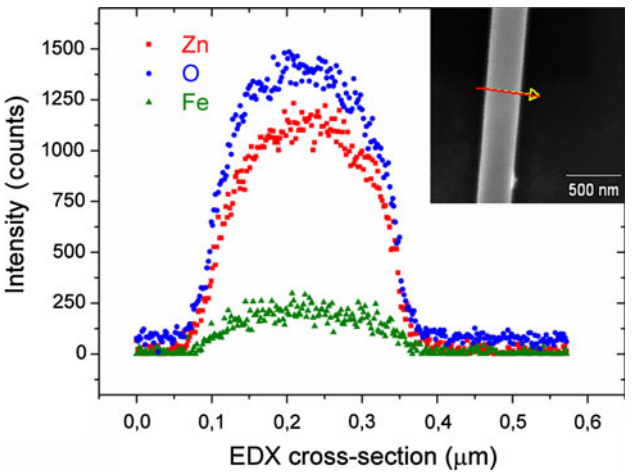

Fig. 5 The EDX signal for Zn, O and Fe atoms across Fe doped ZnO nanofiber. Homogenous distribution of Fe atoms is proved

In Fig. 6, we show a SEM image and a corresponding panchromatic CL map obtained on Fe doped NFs. We find that the light is emitted uniformly from all the fibers. CL (see inset to Fig. 6c) and photoluminescence spectra (not shown) consists of two emission bands. One, centered around 400 nm, is related to the interband recombination. The other one centered around 600 nm is a defect band. It is present in both doped and undoped fibers and most probably originates from oxygen vacancies [34].

In Fig. 7, we present magnetization dependence on magnetic field measured at various temperatures for Fe doped nanofibers oriented along the applied field in the magnetometer. Hysteresis loops are clearly seen up to room temperatures (see inset in Fig. 7) indicating a ferromagnetic coupling present in the system. Both, the magnetic signal and coercive field decreasing on temperature. At room temperature, we still observe a rapid magnetic response to the applied magnetic field. The magnetic signal saturates at above about 5000 Oe. Such a shape of the hysteresis loop clearly indicates that the Curie temperature T_C is substantially larger than 300 K.

At temperatures below 50 K, we find that the magnetic signal does not saturate in magnetic fields below 10 kOe. It is a clear indication that a paramagnetic phase is also present in the NFs. This paramagnetic signal most likely originates from substitution Fe^{2+} and therefore demonstrates a formation of a (Zn,Fe)O ternary alloy.

Figure 8 shows the 30 μm × 30 μm topography and corresponding MFM image (taken at 150 nm lift height) of several randomly oriented Fe doped ZnO fibers, revealing that majority of the fibers interacts magnetically with the MFM probe. Attractive magnetic interactions (dark regions) are clearly visible as shifts in tip resonance frequency as high as few Hz. We find that the magnetic signal is related solely to the fibers and that the Fe ions are evenly distributed along the fibers, but since their magnetization is softer than that of the tip material, only attractive MFM contrast is observed.

The data in Fig. 7, as well as results of zero field cooled (ZFC) and field cooled (FC) measurements (presented in Fig. 9), suggest that the ferromagnetic signal is due to a cooperative behavior typical to a blocked superparamagnet. This indicates that the ferromagnetic coupling takes place only locally. This is not surprising since the structural studies reveal that the NFs consist of nanometer scale crystallites. Their blocked state at room temperature is further corroborated by the presence of a non-zero coercivity of about 60 Oe (see inset in Fig. 7). In order to estimate the volume of magnetic nanoparticles giving rise to the room temperature ferromagnetism, we employ the common formula connecting the value of the blocking temperature T_B with the particle volume V_B and magnetic anisotropy constant K for conventional magnetometry:

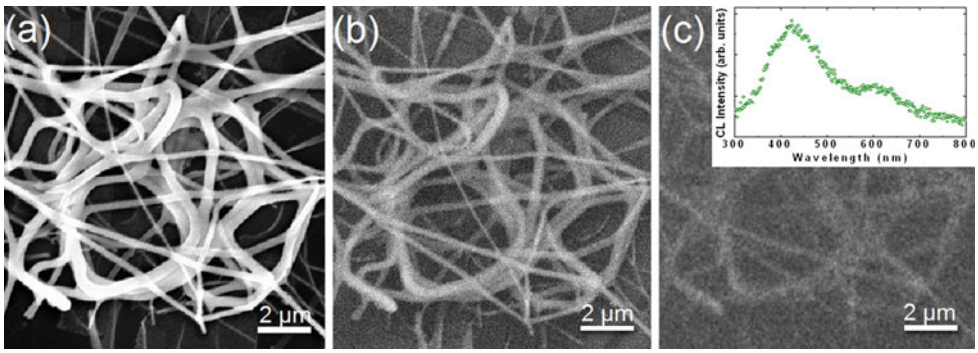

Fig. 6 SEM (**a**), CL panchromatic (**b**) and CL at 400 nm (**c**) images of Fe doped ZnO nanofibers. *Inset*: CL spectrum Fe doped nanofibers

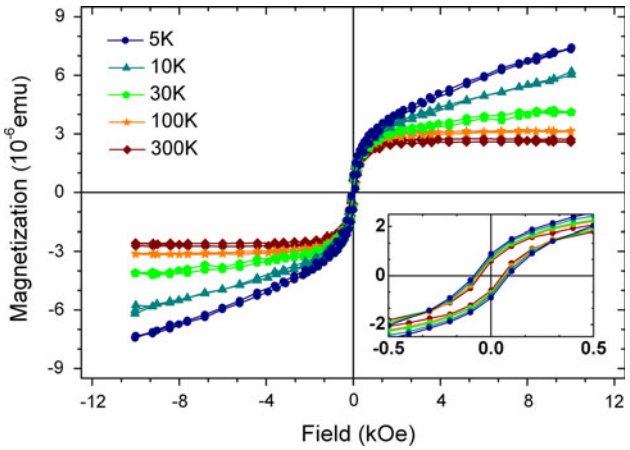

Fig. 7 Effect of magnetization on magnetic field of Fe doped ZnO nanofibers oriented along the applied magnetic field in the magnetometer for various temperatures. Enlargement of the hysteresis loops in the −0.5 to 0.5 kOe magnetic field range (*inset*)

$T_B = 25\ k_B V_B/K$, where k_B is the Boltzman constant. For our material, the anisotropy constant is unknown so we take K in range between 10^5 and 10^6 erg/cm^3, which spans the range of values for bulk crystals (like Fe or its oxides) and nanoparticles with surface enhanced anisotropy. For $T_B = 300$ K, we obtain nanoparticle diameters between 3 and 10 nm. Notably, such particle diameters very well agree with nanocrystal sizes obtained from TEM studies. Interestingly, a weak signal at remanence (approximately ¼ of that in saturation) indicates that the majority of the magnetic nanoparticles in this ensemble is probed along their hard axis. Given that during the measurement the vast majority of the nanofibers was oriented along the magnetic field, we conclude that these nanoparticles have their magnetic easy axes preferentially oriented radially to the axis of the fibers. Moreover, the data collected in Fig. 9 shows a clear peak on ZFC measurement that defines another source of magnetic response in this system with a low blocking temperature of $T_B \cong 20$ K. It points out that there is another kind of magnetic nanoparticles present in the fibers. Using the same arguments as above, we find the corresponding diameters of these nanoparticles to be in the range between 3 and 1 nm for a bulk or the surface-anisotropy enhanced K, respectively.

We do not have all, direct or definitive evidence which mechanism is responsible for the observed ferromagnetism in our NFs. However we are inclined to the following two possibilities. The first one is related to Fe ions substitution in the ZnO matrix. These ions can form a robust ferromagnetic phase mediated by delocalized p-type carriers (holes) [1] or through a superexchange with oxygen vacancies [18]. Since typically ZnO exhibits an n-type conductivity, we conclude that the latter mechanism is the more probable one. Indeed, recently the crucial role of

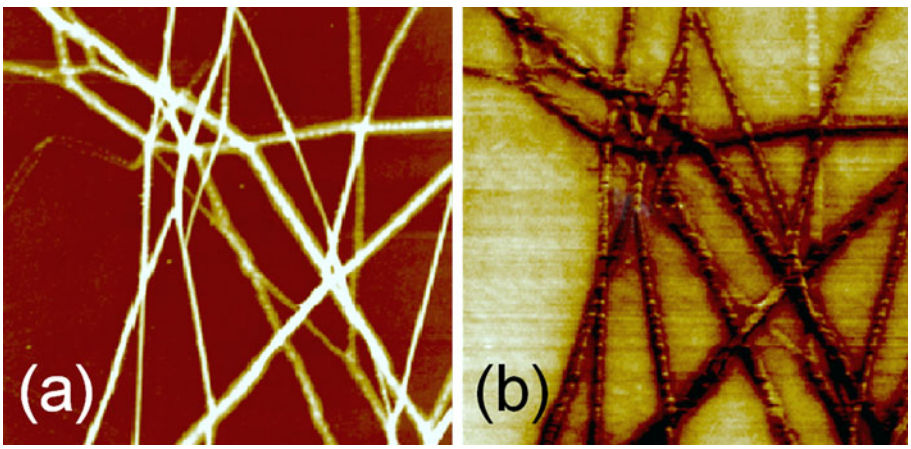

Fig. 8 Comparison of the AFM (**a**) and the MFM (**b**) images of Fe doped ZnO nanofibers. The scanned areas for both images are 30 μm × 30 μm

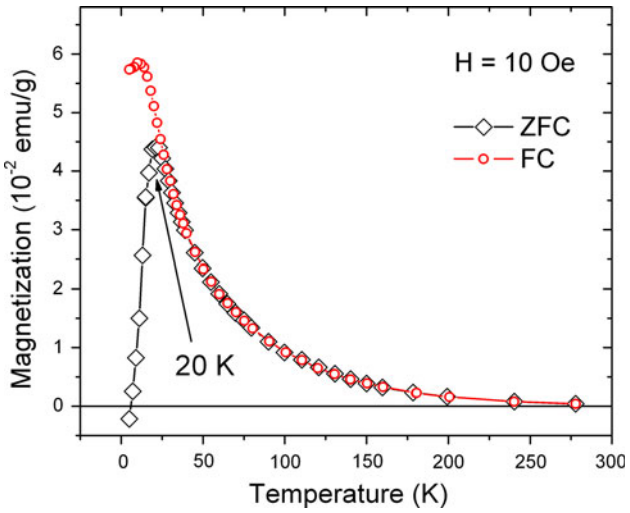

Fig. 9 Zero-field-cooled and field-cooled magnetization as a function of temperature for Fe doped ZnO nanofibers

oxygen vacancies in appearance of the ferromagnetic phase has been proved experimentally [18]. We note that during the calcinations process the presence of carbon ions from precursor substances facilitate the formation of oxygen vacancies in our samples. The second possible explanation is related to a nanoscale phase separation responsible for the presence of Fe-rich magnetic nanoparticles [35]. These particles can take form of α-Fe, various Fe-oxides and/or condensed (Zn, Fe) O. These particles can generate a strong ferromagnetic signal and remain not detected by our structural characterization methods.

4 Conclusions

In conclusion, we developed a fabrication method, which allows us to obtain nanofibers exhibiting ferromagnetism at room temperature. By electrospinning and calcination, we produce about 200 nm in diameter Fe doped ZnO fibers of virtually infinite length, build of about 4.5 nm crystallites oriented with 001 crystal axis perpendicular to the fiber axis. We demonstrate that some of the Fe atoms substitute Zn in the ZnO matrix and give rise to a paramagnetic signal at low temperatures. Incorporating 10% Fe ions does not modify the wurtzite crystal structure of the host ZnO. While the exact origin of the room temperature ferromagnetism remains unknown, we suggest that it is either due to a mechanism mediated by presence of oxygen vacancies or related to small precipitates of ferromagnetic phases of iron. Importantly, compared to previously reported Co and Mn doped ZnO based semiconductors, the synthesized material is a good candidate for biologically compatible therapeutic and diagnostic applications.

Acknowledgments The research was partially supported by the European Union within European Regional Development Fund, through Grant Innovative Economy (POIG.01.01.02-00-008/08) and by the Ministry of Science and Higher Education (Poland) through Grant No. N518 424036 and No. N515 015 32/0997.

References

1. Dietl T, Ohno H, Matsukura F, Cibert J, Ferrand D (2000) Science 287:1019–1022
2. Venkatesan M, Fitzgerald CB, Coey JMD (2004) Nature 430:630
3. Coey JMD, Venkatesan M, Fitzgerald CB (2005) Nat Mater 4:173–179
4. Seshadri R (2005) Curr Opin Solid State Mater Sci 9:1–7
5. Yang JH, Zhao LY, Zhang YJ, Wang YX, Liu HL (2008) Cryst Res Technol 43(9):999–1003
6. Risbud AS, Spaldin NA, Chen ZQ, Stemmer S, Seshadri R (2003) Phys Rev B 68:205202
7. Prellier W, Fouchet A, Mercey B, Simon Ch, Raveau B (2003) Appl Phys Lett 82:3490–3492
8. Lim S-W, Hwang D-K, Myoung J-M (2003) Solid State Commun 125:231–235
9. Lee H-J, Jeong S-Y (2002) Appl Phys Lett 81:4020–4022
10. Sati P, Hayn R, Kuzian R, Régnier S, Schäfer S, Stepanov A, Morhain C, Deparis C, Laügt M, Goiran M, Golacki Z (2006) Phys Rev Lett 96:017203
11. Liu H, Yang J, Zhang Y, Yang L, Wei M, Ding X (2009) J Phys: Condens Matter 21:145803
12. Hong NH, Sakai J, Brizé V (2007) J Phys: Condens Matter 19:036219
13. ACh Mofor, El-Shaer A, Bakin A, Waag A (2005) Appl Phys Lett 87:062501
14. Sundaresan A, Bhargavi R, Rangarajan N, Siddesh U, Rao CNR (2006) Phys Rev B 74:161306R
15. Kim JH, Kim H, Kim D, Yoon SG, Choo WK (2004) Solid State Commun 131:677–680
16. Yoon SW, Cho S-B, We SC, Yoon S, Suh BJ (2003) J Appl Phys 93:7879
17. Lee E-C, Chang K (2004) J Phys Rev B 69:085205
18. Samariya A, Singhal RK, Kumar S, Xing YT, Alzamora M, Dolia SN, Deshpande UP, Shripathi T, Saitovitch EB (2010) Mater Chem Phys 123:678–684
19. Cho YC, Kim S-J, Lee S, Kim SJ, Cho CR, Nahm H-H, Park CH, Jeong K, Park S, Hong TE, Kuroda S, Jeong S-Y (2009) Appl Phys Lett 95:172514
20. Huang Z-M, Zhang Y-Z, Kotaki M, Ramakrishna S (2003) Comp Sci Technol 63:2223–2253
21. Li D, Xia Y (2004) Adv Mater 16(14):1151–1170
22. Ramaseshan R, Sundarrajan S, Jose R, Ramakrishna S (2007) J Appl Phys 102:111101
23. Wu H, Lin D, Zhang R, Pan W (2008) J Am Ceram Soc 91(2):656–659
24. Baranowska-Korczyc A, Sikora B, Zaleszczyk W, Nowicka A, Fronc K, Wojciechowski T, Dziawa P, Knoff W, Gas K, Paszkowicz W, Szuszkiewicz W, Świątek K, Kłopotowski Ł, Sobczak K, Dłużewski P, Karczewski G, Wojtowicz T, Bujak J, Elbaum D (2009) ICFSI-12 in Weimar, abstract-book 302
25. Park J, Kim SS (2009) J Am Ceram Soc 92(8):1691–1694

26. Yang X, Shao C, Guan H, Li X, Gong J (2004) Inorg Chem Commun 7:176–178
27. Ren H, Ding Y, Jiang Y, Xu F, Long Z, Zhang P (2009) J Sol-Gel Sci Technol 52:287–290
28. Pan F, Song C, Liu XJ, Yang YC, Zeng F (2008) Mater Sci Eng R 62:1–35
29. Li Z, Yang R, Yu M, Bai F, Li Ch, Wang ZL (2008) J Phys Chem C 112:20114–20117
30. Gopikrishnan R, Zhang K, Ravichandran P, Baluchamy S, Ramesh V, Biradar S, Ramesh P, Pradhan J, Hall JC, Pradhan AK, Ramesh GT (2010) Nano-Micro Lett 2(1):31–36
31. Gupta AK (2005) Biomaterials 26(18):3995–4021
32. Li D, Wang Y, Xia Y (2003) Nano Lett 3(8):1167–1171
33. Data Base: JCPDS, file 36-1451
34. Cheng W, Ma X (2009) J Phys: Conf Ser 152:012039
35. Bonanni A, Dietl T (2010) Chem Soc Rev 39:528–539